ACS APPLIED MATERIALS & INTERFACES

Research Article

www.acsami.org

A Novel Dry Chemical Path Way for Diene and Dienophile Surface Functionalization toward Thermally Responsive Metal–Polymer Adhesion

Maryline Moreno-Couranjou,*[,†] Anton Manakhov,[†,‡] Nicolas D. Boscher,[†] Jean-Jacques Pireaux,[‡] and Patrick Choquet[†]

[†]Science and Analysis of Materials Department, Centre de Recherche Public-Gabriel Lippmann, 41 rue du Brill, Belvaux L-4422, Luxembourg

[‡]Centre de Recherche en Physique de la Matière et du Rayonnement (PMR), University of Namur (FUNDP), 61 rue de Bruxelles, Namur B-5000, Belgium

ABSTRACT: In this paper, we report a new and easily up-scalable dry chemical method to functionalize with diene and dienophile groups a large range of surfaces, such as metal, polymer, or glass, and we demonstrate the potentiality of this technique to realize thermally responsive adhesion between these materials. A complete and extensive surface chemistry analysis of the grafted surfaces, based on the deposition of an anhydride-rich thin plasma polymer layer by using an atmospheric pressure dielectric barrier discharge (DBD) plasma process, and its subsequent gas phase aminolysis reaction with specific diene or dienophile compound is discussed. The optimization of the assembling condition for these tailored surfaces has led to achieve a Diels–Alder adhesion force up to 0.6 N/mm at ambient temperature, which can be reduced by a factor of 50 when the retro Diels–Alder is ignited at a heating temperature around 200 °C. The study of the failure interface produced after peeling tests is presented and a mechanism of failure is proposed, based on forensic analyses involving surface analytical techniques such as XPS, ToF-SIMS, and SEM combined to AFM analyses for the retrieving of chemical and morphological information.

KEYWORDS: *stimuli-responsive materials, functional coatings, surface modifications, plasma polymerization, thermally responsive adhesion*

1. INTRODUCTION

Because of environmental issues that will be more and more severe in future decades, many industrial sectors such as electronics, transport, or packaging are showing a growing interest in using smart or stimuli-responsive materials such as reversible adhesive systems offering the possibility of easily disassemble or selectively remove manufacturing pieces for maintenance, replacing, or recycling.[1−7] Considering reversible adhesion, different systems have been developed in the past, for example, by incorporating magnetic or electrically conductive micro- or nanoparticles in a shape memory polymer or by exploiting the chemical Diels–Alder (DA) reaction. This latter method seems very attractive and promising as the bonds created are strong covalent chemical linkages that break at high temperature but can reform when the temperature is lowered. Aubert et al. have already developed this kind of original thermal sensitive adhesive and successfully applied it to numerous metals and some foams and polymers.[8] However, an improvement of the method, which will consist of the direct diene and dienophile functionalization of two solid surfaces, could find a larger number of applications.

Recently, two main strategies have been developed to functionalize solid surfaces of different natures. In a first step, methods relying wholly on wet chemical treatments based on self-assembled monolayer (SAM) growth, silylation, or electrochemical reduction reactions have been explored. SAMs have been successfully utilized for the realization of dienophile[9−12] and diene[12] surface functionalization mainly on gold surfaces with the creation of thiol metal bonds. However, such specific groups containing thiol-based molecules do not tend to be commercially available and thus required their custom synthesis. Moreover, this method presents an additional disadvantage in the fact that the thiolate linkages are vulnerable to oxidation and desorption from the gold surface.[13] The silylation technique has also been studied.[14,15] Zhang et al. reported the strong DA adhesion bonding of two functionalized Si wafers annealed for 5 h at 200 °C, with bonding strength up to 1.78 MPa. The chemical grafting was based on a multistep procedure involving the hydroxylization and aminosilylation of the wafers with their subsequent reaction with 2-furaldehyde or maleic anhydride compounds.[15] Maleimide-functionalized gold surfaces were also elaborated by combining the electrochemical reduction of 4-carboxybenzene-diazonium tetrafluoroborate leading to the grafting of benzoic acid moieties and their subsequent activation with 2-ethoxycarbonyl-1,2-dihydroquinoline in order to promote the reaction with first 1,3-diaminopropane and then N-(2-carboxyethyl) maleimide.[16] The substrate-specific and the complex multistep chemistries of these first presented strategies have led to the development of alternative grafting methods based on chemical vapor deposition (CVD) techniques. For example, furan-ring surface functionalization has been achieved by initiated (iCVD) or by

Received: May 16, 2013
Accepted: July 15, 2013
Published: July 15, 2013

ACS Publications © 2013 American Chemical Society

dx.doi.org/10.1021/am401851y | ACS Appl. Mater. Interfaces 2013, 5, 8446–8456

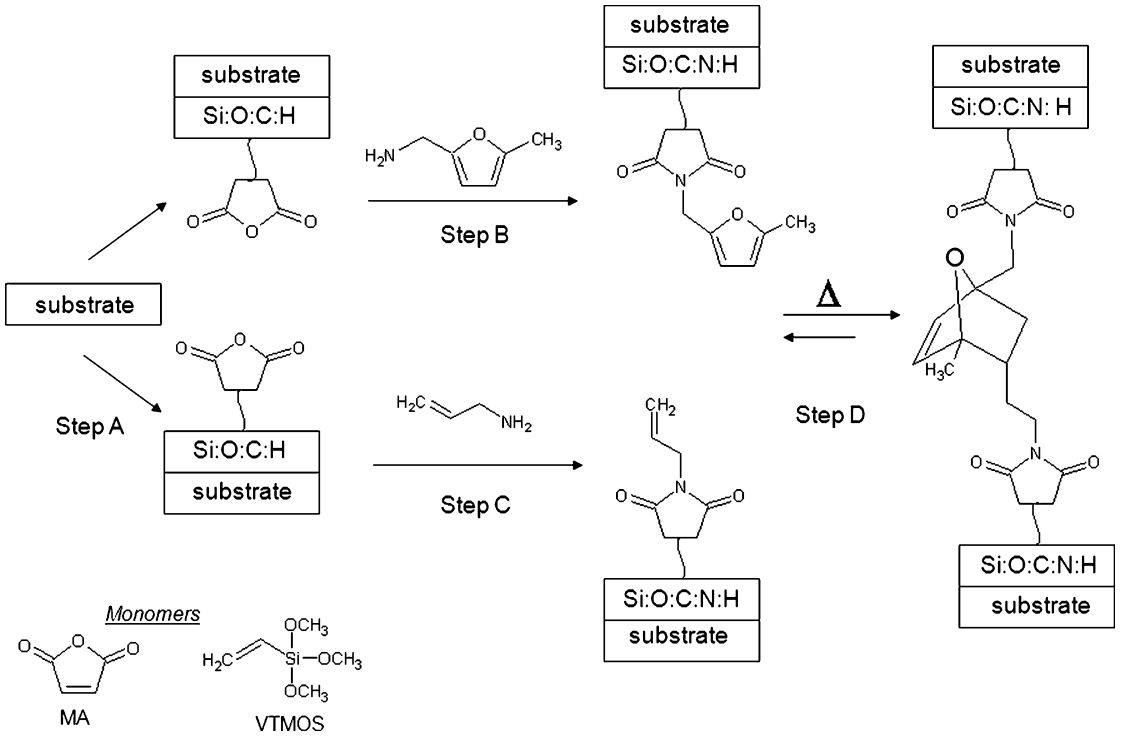

Figure 1. Schematic of the novel dry atmospheric process for diene and dienophile surface functionalization.

plasma-enhanced chemical vapor deposition (PECVD) of furfuryl methacrylate.[17,18] Despite being a solvent-free process to form films under mild conditions, iCVD presents the drawbacks of requiring the use of a low vacuum deposition reactor and of specific substrate surface preparation to ensure the good thin film adhesion. To circumvent these limitations, researchers have further studied the potentialities of PECVD processes.

Hence, Roucoules et al. have recently reported a DA reaction between two functionalized aluminum surfaces with a relatively low peel strength value reaching 0.19 N/mm for more than 10 heating/cooling cycles.[19] In this case, the chemical grafting was achieved by combining low-pressure plasma polymerization of maleic-anhydride and wet chemical treatments including the complete multistep custom synthesis of the cyclopentadienyl-n-undecanamine used as diene.[12]

In this work, the elaboration of a thermally responsive strong adhesive system is targeted. For that purpose, a new dry chemical pathway for the synthesis of diene- and dienophile-functionalized surfaces has been developed based on atmospheric plasma polymerization and chemical gas phase reaction with commercial compounds. The contribution is divided into three parts.

In the first one, the general developed chemical pathway is described. In a second part, the successful diene and dienophile graftings on three different substrates (aluminum, PEN, and Kapton) are confirmed by combining FT-IR and XPS analyses along with the morphology of the coatings thanks to SEM observations. In particular, a XPS curve fitting methodology is presented in order to estimate the amount of grafted dienophile and diene groups. The reactivity of the dienophile functionalized layers is further evaluated according to a Diels–Alder reaction in solution. This section will indeed suggest that our strategy is quite general, and could be applied to any type of substrate pair. In a third part, the optimized contact conditions, i.e., pressure, temperature, and contact time under the heat press, leading to DA adhesion property are presented for two different laminate materials: the PEN-PEN case will serve to demonstrate our methodology for delaminating the materials and study the exposed interfaces, whereas the Al-Kapton laminate will be studied in more detail, including the demonstration of the influence of the temperature on the metal–polymer adhesion strength, i.e., the thermal response of the system.

2. EXPERIMENTAL SECTION

2.1. Deposition of Anhydride-Rich Plasma Polymer Coatings and Materials. MA-VTMOS plasma copolymer layers were deposited onto metallic or polymeric substrates by using an atmospheric pressure dielectric barrier discharge plasma process (DBD-Lux 600) developed by the Fraunhofer Institute for Surface Engineering and Thin Films IST, Braunschweig, Germany. The plasma was generated using a Corona generator 7010R (SOFTAL electronic GmbH) delivering a continuous or pulsed sinusoidal voltage signal, whose frequency was fixed at 10 kHz. The plasma was ignited between two flat parallel high voltage electrodes (1.5 × 30 cm^2) covered with alumina and a moving stage as grounded electrode and supporting the material to be treated. The gap between the electrodes was fixed to 1 mm. A 10 mm s^{-1} table speed was used, while the number of runs was adjusted to deposit a 20 nm thick layer, according to the deposition rate estimated for each material nature. Argon (Air Liquide, 99.999%) was used as a process and carrier gas for all experiments. Prior to the deposition experiment, the aluminum and polymeric substrates were cleaned and activated into an Ar:O_2 (95%:5%) or N_2:O_2 (95%:5%) AP-DBD plasma discharge for 60 s, respectively. The two precursors, VTMOS and MA (Sigma Aldrich, 98%), were injected into the reactor using a double bubbler system. The argon flow rates through the VTMOS and MA bubblers were kept constant to 0.25 and 14.8 L min^{-1}, respectively. Hence, the precursor concentration in the gas phase was 6.3 × 10^{-6} mol L^{-1} for both monomers.

One-millimeter-thick aluminum foils of 1015-H14 alloy were purchased from Forward Metals and polished to reach a 4 nm Ra value. The substrates were subsequently cleaned in hexane (≥99%,

Table 1. Infrared Assignments of MA-VTMOS Plasma Layers and Corresponding Derivatized Surfaces with 5-Methylfurfurylamine (MFA) or Allyl Amine

peak position (cm^{-1})	assignment	MA-VTMOS plasma layer	plasma layer + MFA	plasma layer + allyl amine
3500−3200	carboxylic acid or secondary amide O−H stretch N−H stretch (1 band)	*	*	*
3090−3075	alkene, vinyl C−H stretch			*
2970−2920	methoxy, CH_3−O C−H asymmetric stretch	*		
2850−2700	aldehyde C−H stretch (1 band)	*		
2830 ± 10	CH_3−O C−H symmetric stretch	*		
1870−1845	cyclic anhydride C═O stretch	*		
1800−1775	cyclic anhydride C═O asymmetric stretct	*		
1790−1735 1750−1680	cyclic Imide C═O stretches (2 bands)		* (after annealing)	* (after annealing)
1680−1630	secondary amide C═O stretch		*	*
1740−1700 very strong	carboxylic acid C═O stretch	*	*	*
1730 ± 10	C═O stretch saturated aldehyde	*		
1570−1515 strong	secondary amide N−H in-plane bend		*	*
1470−1440	CH_3−O CH_3 umbrella mode	*	*	
1440−1395 weak	carboxylic acid combination C−O stretch and OH deformation	*	*	*
1610−1360 strong, sharp bands	ring skeleton heteroaromatic compound		*	
∼ 1190	Si-OCH_3 CH_3 rocking vibration	*		
1310−1210 strong	cyclic anhydride C−O−C stretch	*		
1190−990 medium or strong	furan ring CO-C stretch		*	
1090−1010	Si−O−Si, Si−O stretch	*	*	*
990−725 (generally strong)	furan ring CH deformation, out of plan vibration		*	
930−932	Si−OH stretching Al−O (substrate)	*	*	*
800−810 cm^{-1}	SiO_2, Si−O bending	*	*	*

Sigma-Aldrich), acetone (≥99.9%, Sigma-Aldrich) and ethanol (≥99.8%, Sigma-Aldrich) ultrasonic baths and dried under a nitrogen flux. Polyethylenenaphtalate (PEN Q65F) and polyimide (Kapton NH grade) foils were purchased from DuPont. The foils were cleaned in ultrasonic baths of acetone and ethanol and dried under a nitrogen flux. Maleic anhydride (MA) (99%, Merck), vinyltrimethoxysilane (VTMOS) (98%, Sigma Aldrich), allyl-amine (99%, Sigma-Aldrich), 5-methylfurfurylamine (97%, Sigma-Aldrich), 5-bromo-2-furaldehyde (99%, Merck), and toluene (for synthesis >99%, Merck) were used as received.

2.2. Assembling of the Substrates and Adhesion Force Measurements. The assembling of the substrates was done using the Micro-Mold 100 kN heating press (JBT Engineering, UK). Adhesion force measurements were carried out using a Tinius Olsen H1KT instrument (Benelux Scientific) with a 5 $mm \cdot min^{-1}$ peeling speed in a 90 or 180° configuration for two flexible or solid-flexible substrate assemblies, respectively.

2.3. Surface Characterization. X-ray photoelectron spectroscopy (XPS) analyses were carried out using an Axis Ultra DLD (Kratos Analytical Ltd.) instrument equipped with a monochromatic Al Kα X-ray source ($h\upsilon$ = 1486.6 eV) and an electron flood gun for insulating substrate analyses. These measurements were carried out at a 20 eV pass energy, an X-ray power equal to 150 W, on a sample area of approximately 0.7 × 0.3 mm^2. The relative sensitivity factors were provided by the manufacturer and equal to 0.278, 0.78, 0.328, 0.477, 1.279 for carbon (C 1s), oxygen (O 1s), silicon (Si 2p), nitrogen (N 1s), and bromine (Br 3p), respectively. The experimental uncertainty related to the XPS surface elemental composition is around 1 at %. The error limit related to the relative proportion of the different carbon functionalities is around 2% considering both the errors related to the C1s curve fittings and the carbon quantification.

Fourier-transform infrared (FTIR) analyses in the Attenuated Total Reflection (ATR) or grazing angle (GR) mode were carried out with a Bruker Hyperion 2000 microscope equipped with a Ge-crystal-objective associated with a mercury−cadmium−telluride (MCT) detector cooled with liquid nitrogen. Spectra were acquired with 100 scans in the range from 4000 to 500 cm^{-1}.

Static secondary ions mass spectrometry (SIMS) analyses were performed with a Time-of-Flight (ToF)-SIMS V instrument (ION-TOF GmbH, Muenster, Germany) equipped with a Bi liquid metal ion gun. All spectra were collected with 25 keV Bi_3^+ primary ion beam and the ion dose has been kept below the static SIMS limit. ToF-SIMS data was collected using the high mass resolution mode (mass resolution power >5000, lateral resolution ∼1 μm). Data was recorded by scanning the primary ion beam over an analysis area of 500 × 500 μm^2. Charge compensation of the samples was accomplished using a pulsed low-energy electron flood gun.

Scanning electron microscopy (SEM) was performed using the field-emission SEM SU-70 (Hitachi) at 15−20 kV.

Atomic force microscopy (AFM) measurements were performed in ambient air in the Tapping Mode using a PicoSPM LE with a large scanner controlled by the Pico Scan software (Agilent, Santa Clara, CA, USA). Topographic images were recorded at a scanning rate of 1 Hz using a standard unmodified silicon tip (AppNano ACT model).

3. RESULTS AND DISCUSSION

The path-way to synthesize the diene and dienophile functionalized surfaces is schematically presented in Figure 1. It is based on the combination of two dry atmospheric techniques, which can be realized in the same deposition chamber at the atmospheric pressure and is also appropriate to treat very large surfaces. Hence, in step A (Figure 1), a smooth and anhydride rich-coating is deposited on the substrates by using a pulsed anhydride maleic (MA)-vinyltrimethoxysilane (VTMOS) plasma copolymerization process based on the dielectric barrier discharge technology. During step B, an aminolysis gas phase reaction is performed at ambient conditions between the anhydride functionalized layer and the primary amino group carried out by the selected diene compound, i.e., 5-methylfurfuryl amine. Interestingly, because of its descendant from renewable sources, the use of this furan derivative allows to promote sustainable developments in

materials science.[20] Similarly, the dienophile grafting is achieved thanks to the gas phase reaction between the anhydride rich layer and the amino group of a dienophile molecule, i.e., allyl amine. The strong Diels–Alder covalent bond is then created by placing the coated surfaces in contact under controlled pressure, temperature, and duration conditions (Figure 1, step D).

In the next three sections of the second part of the paper, we report more details on the elaboration and the characterizations of each functionalized surface.

3.1. Elaboration of Highly Chemically Reactive Anhydride-Rich and Smooth Coatings. Polymer surfaces containing anhydride groups are widely sought for their high chemical reactivity notably providing anchoring sites for further molecule grafting based on a nucleophilic attack by amine-or hydroxyl-terminated moieties to produce amides/imides and ester linkages, respectively.[21] In a previous paper, we reported on the ability of an atmospheric pressure DBD process to fine-tune the chemistry and morphology of anhydride-containing films by programming the electrical discharge parameters (i.e., power and duty cycle).[22] The films are obtained from a pulsed MA-VTMOS plasma copolymerization where MA provides the anhydride functionality and VTMOS stabilizes the overall polymer network: indeed the creation of a Si–O–Si skeleton results from the hydrolysis and condensation of the initial methoxysilane groups. For this work, the electrical parameters for the coating deposition were selected to elaborate anhydride rich and smooth coatings, limiting the anchoring mechanism between the two functionalized surfaces. One requisite condition for the Diels–Alder reaction is the coplanarity of the diene and dienophile molecules to ensure efficient molecular orbital interactions. In the past, Roucoules et al. built their DA system by grafting a diene-terminated molecule containing a C_4 long alkane chain. Hence, the diene is kept away from the surface and especially gains in mobility/conformal orientation.[12,19] In opposition, as reported in figure 1, our commercially available diene molecule is short, and presents poor conformal freedom. Hence, in order to promote diene and dienophile coplanar interactions, a statistical approach has been exploited based on a high molecule grafting density, thus requiring high anhydride density.

Using a dissipated power of 2.3W/cm^2 and pulsed MA-VTMOS plasma discharges (t_{on} = 10 ms and t_{off} = 40 ms) coatings with optimum anhydride group retention were deposited as confirmed by Fourier Transform infrared analysis (Table 1). Indeed, the characteristic cyclic anhydride absorbance peaks were detected: asymmetric and symmetric C=O stretching and C–O stretch vibrations. Additionally, it is worth noting that the VTMOS structure is also well retained during the plasma polymerization as the following characteristic peaks initially present in the monomer are detected: CH asymmetric and symmetric stretch from CH_3O, CH_3 umbrella mode from CH_3O and CH_3 rocking vibration from Si-OCH_3.

In accordance with the FT-IR results, the XPS C 1s core level peaks were fitted with five components, namely (i) hydrocarbon and carbon singly bonded to silicon (C–C/C–Si ~285.0 eV used for the calibration), (ii) carbon singly bonded to an anhydride group (C–C(O)–O ~285.7 eV), (iii) carbon singly bonded to oxygen (C–O ~286.5 eV), carbon doubly bonded to oxygen (C=O ~287.8 eV), and (iv) anhydride/carboxylic groups (O–C=O ~289.3 eV). The full width at half maximum (FWHM) and the Gaussian–Lorentzian (G/L) ratio values were fixed at 1.8 ± 0.05 eV and 30% respectively. An additional constraint has been included in the curve fitting, to ensure the equality of the peak area contributions of the C*–C(O)–O and O–C=O chemical groups. Hence, the XPS study of a plasma-coated aluminum foil revealed the presence of 12 at % O–C=O functions. Similar XPS elemental concentrations and C1s environments have been found for coatings deposited on Kapton and PEN foils, giving a O–C=O content around 10 and 11 at % respectively. These measurements highlight that with our chosen experimental conditions, the substrate nature does not strongly influence the plasma layer chemistry.

Finally, according to SEM observations (not shown), we have verified that whatever the substrate (metal or polymer one), all the coatings present a homogeneous morphology and are free of cracks.

3.2. Elaboration and Characterization of Dienophile Functionalized Surfaces. As schematized in Figure 2, the gas phase reaction of the MA-VTMOS plasma polymer-deposited films with allylamine was carried out at atmospheric pressure in a closed flask containing 0.3 mL of allylamine. After 1 h of exposure, the dienophile-functionalized surface was removed and placed in an oven at 120 °C for 2 h under ambient conditions to transform the amide groups into more stabilized cyclic imide groups.

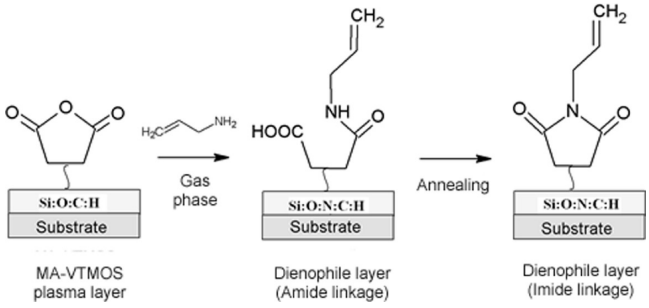

Figure 2. Scheme of the dienophile surface functionalization.

After reaction of the MA-VTMOS plasma copolymer layer with allyl-amine, FT-IR analyses confirmed the anhydride ring-opening to yield amide and carboxylic groups. Indeed, the initial anhydride peaks visible at 1855 and 1783 cm^{-1} disappeared, whereas two new peaks appeared at 1646 and 1563 cm^{-1} in relation to the C=O and N–H vibrations of a secondary amide (Figure 3a, b). In parallel, an increase in the COOH band intensity around 1730 cm^{-1} was observed. At this stage, it was also possible to detect a peak at 3030 cm^{-1} that might be attributed to the C–H asymmetric band vibration of the vinyl compound, thus confirming the good alkene grafting. After annealing, the cyclic imide bond formation was confirmed with the presence of the C=O vibrations at 1772 and 1731 cm^{-1} (Figure 3c). Interestingly, amide spectral features were also observed, suggesting that the imidization process occurred just at the surface (and not in the complete layer thickness). Finally, the appearance of nitrogen in the layer estimated at 5.0 at % from the XPS measurements (Table 2) is in accordance with the grafting of the dienophile molecule.

The XPS C1s curve fitting of the dienophile functionalized layer allowed to determine the different carbon environments and also to estimate the amount of grafted alkene group. The Si 2p position defined in the original MA-VTMOS functionalized layer has been used for calibration of the binding energy scale, as the aminolysis reaction should not affect the Si environment

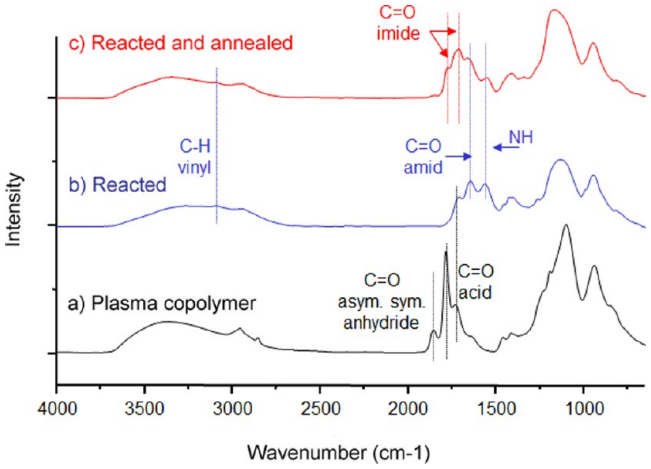

Figure 3. ATR-IR spectra of MA-VTMOS plasma copolymer layer (a) as deposited on aluminum, (b) after the reaction with allyl-amine (amide linkage), and (c) after the annealing step (imide linkage).

Table 2. XPS Elemental Compositions of Dienophile Functionalized and Derivatized Layers

samples	XPS elemental concentration (at %)				
	C	O	Si	N	Br
dienophile functionalized aluminum	59	30	6	5	
dienophile functionalized PEN	53	36	8	3	
derivatized MA-VTMOS plasma layer	57	35	7	1	
derivatized dienophile layer	58	31	6	3	2

(Figure 2). Figure 4 presents the superposition of the XPS C1s spectra of the copolymer layer before and after the aminolysis

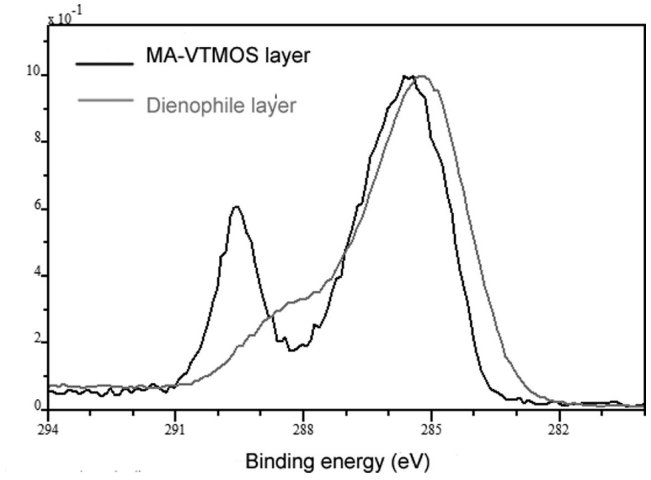

Figure 4. Superposition of the XPS C1s spectra of the MA-VTMOS plasma layer as deposited on aluminum and the corresponding dienophile functionalized layer (energy calibration using the Si2p peak).

reaction: it clearly allows to highlight the strong modification of the C1s environment with the disappearance of the C(O)O peak and the appearance of a new contribution at a binding energy lower than 285 eV that might be attributed to vinyl groups.

The XPS C1s curve analysis of the dienophile-functionalized layer on the aluminum substrate (Table 3) reveals 6 different

Table 3. XPS C1s Curve Fitting Results Obtained from the Dienophile Functionalized Aluminum and PEN Substrates

binding energy (eV)	functional group	proportion relative to total carbon amount (at %)	
		dienophile functionalized aluminum	dienophile functionalized PEN
284.1–284.2	C═C vinyl; alkene	10	6
285.0	C–C	23	24
285.7–285.8	C*–C(O)–N amide	5	4
286.5–286.6	C–O/C*–NH–C(O) amide	12	10
287.7–287.8	C═O/O═C–N amide	5	2
288.8–288.9	O═C–N–C═O imide	5	7

functionalities: carbon doubly bonded to a carbon (C═C ∼284.1 eV), hydrocarbon (C–C ∼285.0 eV), carbon singly bonded to an amide group (C*–C(O)–N ∼285.7 eV), carbon singly bonded to oxygen or singly bonded to an amide nitrogen (C–O/C*–NH–C(O) ∼286.7 eV), carbon doubly bonded to an oxygen or amide group (C═O/O═C–N ∼ 287.7 eV) and imide bond (O═C–N–C═O ∼288.8 eV). The FWHM and G/L ratio were fixed in the 1.2–1.6 eV range and at 30%, respectively. By taking into account the measured total carbon amount and the C1s curve fitting results, it appears that ca. 10 at % carbon is involved in alkene bonds. This result is in good agreement with the nitrogen concentration estimated at 5 at % (Table 2), as one nitrogen is involved in each grafted alkene group. Moreover, the fact that the relative alkene concentration is not equal to the imide one, but to the imide plus amide relative concentration suggests that the imidization is not 100% effective: as a consequence, dienophile molecules are carried by both amide and imide groups. This hypothesis is fully consistent with the results obtained in the XPS N1s curve fitting (not shown), as both amide (N–C═O) and imide (O═C–N–C═O) contributions are present at 399.9 and 400.7 eV, respectively. Additionally, a third small contribution appears at 402.1 eV that could be assigned to an ammonium salt (NH_3^+) issued from the protonation of the amine group by the carboxylic group created during the amonilysis reaction.[21]

To develop polymer–polymer adhesion based on DA reaction, PEN substrates were also treated according to the developed procedure and the successful dienophile surface functionalization confirmed via XPS analyses. Indeed, the C1s curve fit, reported in Table 3, is composed of different carbon functionalities whose nature and concentration are similar to the ones detected in the dienophile functionalized aluminum. Again, a good correlation is obtained between the estimated grafted alkene group (around 6 at %) and the nitrogen content at the surface (3 at %) (Table 2).

In summary, XPS analysis allows to confirm the grafting of dienophile molecules on both metal and polymer substrates and to estimate their concentration. However, no information can be reported about the potential reactivity of these dienophile groups. With this objective, an interfacial Diels–Alder reaction was carried out. Hence, a freshly prepared dienophile functionalized polished aluminum substrate was immersed in a solution of toluene containing 5-bromo-2-furaldehyde at 0.2 mol L^{-1}. The reaction mixture was heated to reflux for 2 or 4 h. Afterward, the functionalized substrate

surface was washed with toluene and dried under a stream of nitrogen prior to the characterization. The XPS quantification of the present brominate element allowed to estimate the yield of the reaction and thus the availability of the dienophile molecules (Figure 5).

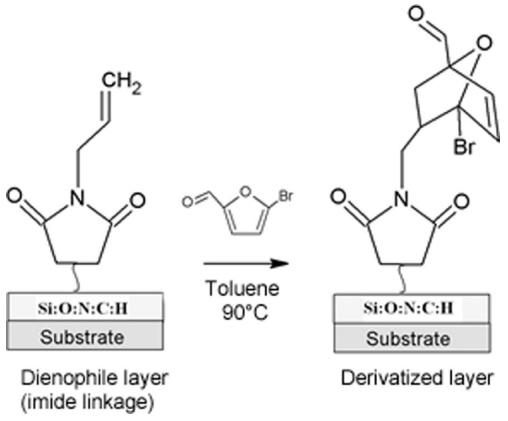

Figure 5. Scheme of the interfacial Diels–Alder reaction in solution involving the dienophile layer and the 2-bromofuraldehyde.

As reported through the XPS results in Table 2, the selectivity of the brominated compound toward the dienophile functionalized surface was confirmed as no Br was detected when a MA-VTMOS plasma layer underwent the DA reaction. One can notice on the appearance of around 1 at %, nitrogen, but this value, close to the limit of sensitivity of the XPS analysis, can be attributed to surface contamination. After the DA reaction, the dienophile derivatized layer presents 2 at % Br and 3 at % N, although according to Figure 5, a 100% yield should lead to the equality between these 2 elements. Nevertheless, considering the XPS sensitivity accuracy, it can be reasonably concluded that the Diels–Alder adduct formation yield is close to 100%.

3.3. Elaboration and Characterization of Diene-Functionalized Surfaces. As schematized in Figure 6, different diene functionalized substrates were elaborated according to an aminolysis gas phase reaction between the MA-VTMOS plasma copolymer deposits and the 5-methyl-furfurylamine (MFA).[23] The reaction was carried out at atmospheric pressure in a closed flask containing 1 mL of the reactant. After 2 h of exposure, the diene-functionalized surface was removed and placed in an oven at 120 °C for 2 h to form stable imide linkages carrying diene groups.

After reaction with MFA, the amide formation was confirmed by the FT-IR analyses (Figure 7). Indeed, the initial anhydride

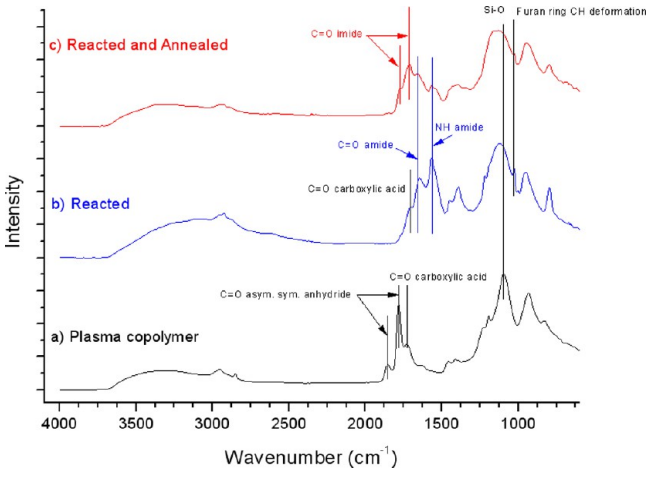

Figure 7. ATR-IR spectra of MA-VTMOS plasma copolymer layer (a) as deposited on aluminum, (b) after reaction with MFA (amide linkage), and (c) after annealing (imide linkage).

peaks visible at 1855 and 1783 cm^{-1} disappeared while two new peaks appeared at 1646 and 1563 cm^{-1}: they are related to the C═O and N–H vibrations of a secondary amide (Figure 7a and b). After the annealing reaction, the cyclic imide bond formation was confirmed with the presence of the C═O vibrations at 1772 and 1731 cm^{-1} (Figure 7c). Finally, the diene functionalization was also quantitatively confirmed by the XPS analysis with the detection of 4 at % nitrogen (Table 4).

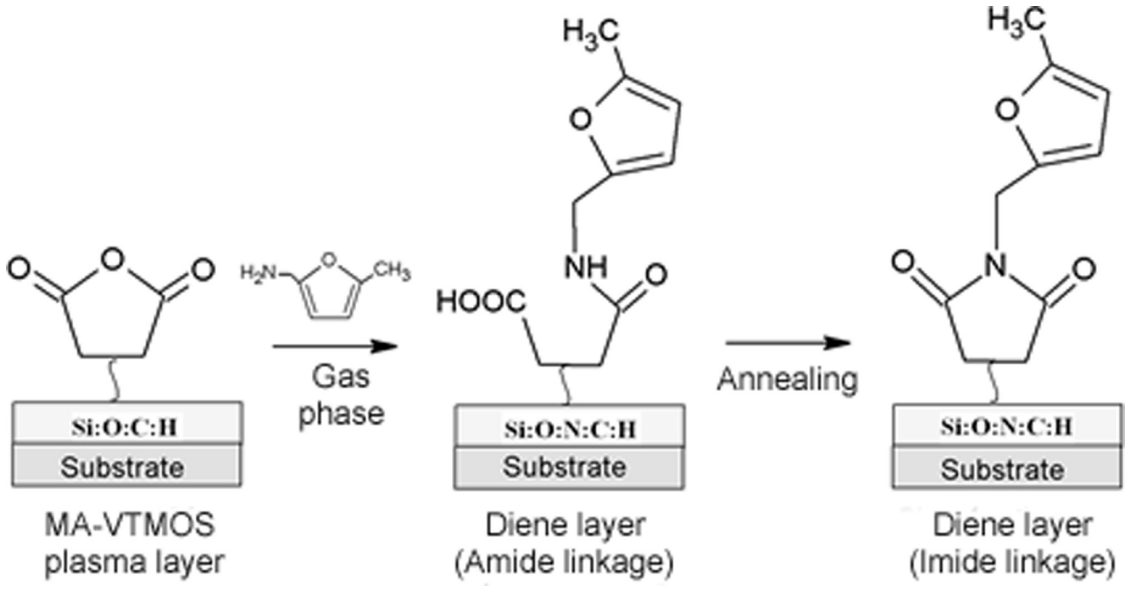

Figure 6. Scheme of the diene surface functionalization.

Table 4. XPS Elemental Concentration and C1s Curve Fitting Results Obtained on Diene-Functionalized Aluminum, Kapton, and PEN Substrates

	XPS elemental concentration (at %)		
element	diene-functionalized aluminum	diene-functionalized Kapton	diene-functionalized PEN
C	56	55	53
O	34	35	36
Si	6	7	8
N	4	3	3

		XPS C1s deconvolution[a] (at %)		
binding energy, eV	functional group	diene-functionalized aluminum	diene-functionalized Kapton	diene-functionalized PEN
284.7	C═C	8	9	8
285.0−285.1	C−C	17	16	17
285.7−285.8	C*−C(O)−N	10	12	9
286.5−286.7	C−O/C*−NH−C(O)	10	7	8
287.7−287.9	C═O/O═C−N	3	4	2
288.8−289.0	O═C−N−C═O	9	8	8

[a]Proportion relative to total carbon amount, at %.

Analysis of the XPS C1s spectra (superposition of the MA-VTMOS plasma layer on aluminum and of the corresponding diene layer, using the same Si2p calibration step) reveals also significant changes (not shown), which are in good agreement with the FT-IR results. An accurate XPS C1s curve fit shows that the C(O)O peak shifts toward lower binding energy at 288.8 eV accompanied with an intensity increase around 287.9 eV: this is clearly related to the conversion of the anhydride groups into imide and amide groups respectively. Moreover, the diene C1s curve fit (Table 4) requests an additional peak around 284.7 eV to be related to the presence of C═C bonds at the surface. Finally, one can also note that the binding energy of the C═C groups from the diene functionalized surface is higher than the one estimated for the alkene group (284.7 eV vs 284.1 eV); this is probably due to the electron withdrawing effect of the oxygen atom from the furan ring of the MFA molecule.

Because of the dominant FT-IR signatures of the PEN and Kapton polymer substrates, it was not possible to investigate their chemical surface modifications by using this technique. But the XPS C1s curve fits (Table 4) reveal that the different carbon functionalities detected are similar, in nature and concentration, to the ones estimated on the aluminum substrate: they allow to conclude to the successful grafting of diene molecules on both PEN and Kapton substrates. Moreover, there is a good coherence between the total nitrogen content (around 3 at %) and the amount of the total carbon involved in the estimated C═C content (i.e., 8 at %).

3.4. Adhesion Properties of Two Functionalized Surfaces. In the first part, we will report on the study of the formation of the PEN-PEN laminates, and then study the interfaces after peeling. The developed procedure will then be used in the second section to investigate in details the Al-Kapton laminates, and to show thermally activated reversible adhesion.

3.4.1. Diels−Alder-Based Polymer−Polymer Adhesion. Diene- and dienophile-functionalized PEN substrates (90 × 25 × 0.1 mm^3) were assembled by using a heating press. The temperature and pressure were varied from 70 to 100 °C and 20 to 70 bar, respectively, whereas the contact time was ranged from 30 min to 4 h. The first assemblies, obtained by using different pressures and temperature and a 30 min fixed contact time, revealed that, whatever the pressure used, no adhesion force was obtained for temperatures under 150 °C. Effectively, adhesive joints were only obtained for assemblies carried out at 150 °C leading to a 60 J/m^2 adhesive strength.

Figure 8 reports the fracture energy, evaluated by 180° peel-tests, of assemblies carried out at a 150 °C fixed temperature,

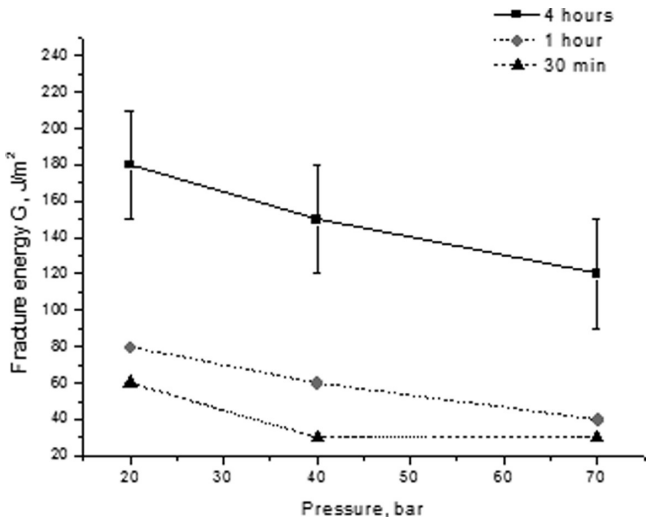

Figure 8. Fracture energy (J/m^2) of diene- and dienophile-functionalized PEN assemblies obtained at different pressure and contact time for a 150 °C fixed temperature.

for different pressure and contact time. It can be clearly observed that irrespective of the pressure, the increase of the contact time favors the adhesion. Hence, the fracture energy can increase up to a factor of 4 when increasing the contact time from 30 min to 4 h. In contrast, the increase of the pressure led to a decrease of the adhesion. This is probably due to the brittleness of the PEN foil, as assembling at higher pressure might induce cracks and damages in the polymer film. The highest fracture energy, 180 J/m^2, was obtained for functionalized PEN assembling carried out at 150 °C, 20 bar during 4 h.

For the selected condition of assembling, laminates of naked PEN, MA-VTMOS-functionalized PEN and two dienophile-functionalized PEN were prepared. Figure 9 reports the evolution of the fracture energy as a function of the peel length obtained for the aforementioned laminates along with

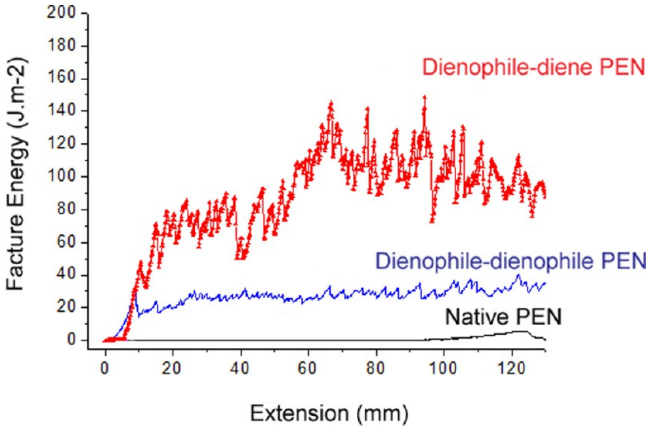

Figure 9. Fracture energy as a function of peel length (extension) for different assemblies realized in the same conditions of 150 °C, 4 h, 40 bar: native PEN (black line), two dienophile-functionalized PEN (blue line), and diene- and dienophile functionalized PEN (red line).

the diene-dienophile assembly. Hence, it can be clearly observed that only diene- and dienophile-functinalized PEN assembly led to high adhesive joints (fracture energy up to 140 J/m^2). Assemblies of two dienophile-functionalized PEN do not lead to adhesion above 30 J/m^2, whereas no adhesion property is achieved for two native PEN laminates, thus excluding any kind of mechanical-based adhesion. Hence, it can be concluded that the developed adhesion property is mainly based on DA chemical adhesion.

After the adhesion test, the diene and dienophile PEN surfaces present multiple cracks (not initially visible) of a few millimeters length aligned perpendicularly to the peeling length: they are highlighted by SEM analysis (Figure 10).

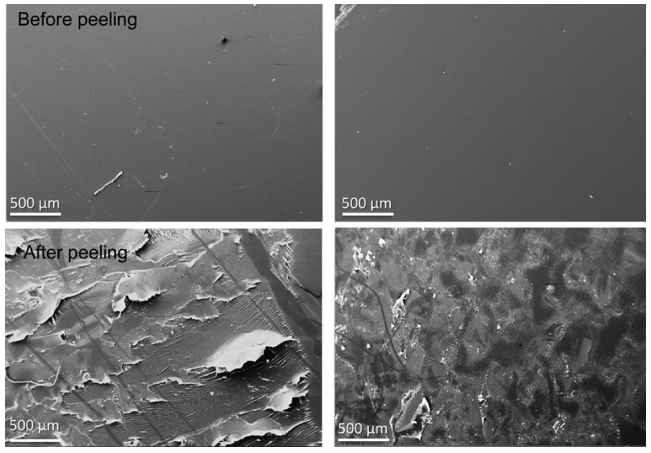

Figure 10. Diene- (left) and dienophile-functionalized (right) PEN substrates before (top) and after (bottom) peeling at ambient temperature.

According to the elemental composition estimated by XPS after peeling (not reported here), the surfaces clearly differ from the original functionalized ones. Indeed, no nitrogen was detected on any surface while an important increase in carbon and oxygen contents, up to 20 and 10 at. % respectively, was observed. Hence, the composition of each peeled interface is quite similar to the PEN one, with however the presence of a small silicon content that can be related to some residue coming from the MA-VTMOS copolymer layer. The XPS C1s spectra shapes of the diene and dienophile surfaces after peeling are clearly similar to the native PEN one. The C1s curve fits required three components, namely: aromatic carbon (C═C ∼284.6 ± 0.1 eV, used for calibration), carbon singly bonded to oxygen (C−O ∼286.5 ± 0.1 eV), and carbon involved in ester bonds (O−C═O ∼288.6−288.9 eV) with FHWM values ranging from 0.9 to 1.3 eV. Additionally, a shake-up satellite around 291.2 eV had to be introduced attesting the presence of PEN aromatic structure.

Hence, according to SEM and XPS analyses, it can be concluded that the major locus of failure originates inside the PEN substrate, revealing that the adhesion strength produced by the DA chemistry is stronger than the cohesive strength in PEN.

The retro-DA reaction occurring at a temperature higher than the DA one, it was not possible to investigate the thermally adhesive response of the functionalized PEN assemblies. To overcome this problem, we have applied the same functionalization strategy on a Kapton and aluminum substrate.

3.4.2. Thermally Responsive Metal−Polymer Adhesion. The peeling at ambient temperature of dienophile and diene functionalized polished aluminum and Kapton substrates assembled according to optimized conditions (60 bar, 175 °C, 4 h) revealed an adhesion force up to 0.6 N/mm. Interestingly, assemblies performed at 200 °C presented poor peel-strength values (around 0.1 N/mm), suggesting the occurrence of some retro Diels−Alder reactions. Finally, although both functionalized surfaces initially presented smooth morphologies, the peeling induces the formation of many cracks on Kapton and defects on aluminum (Figure 11).

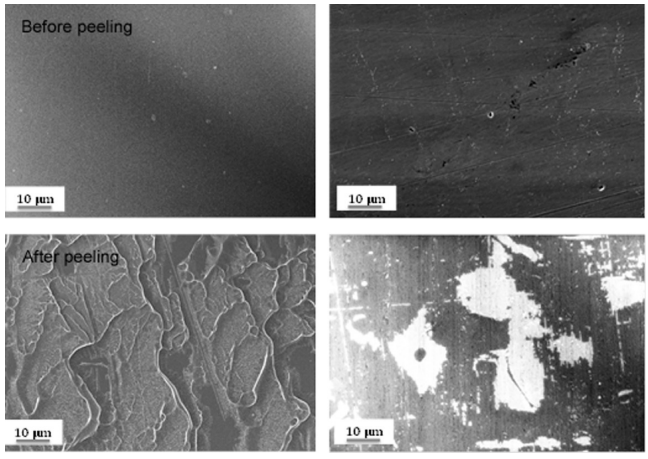

Figure 11. SEM images of diene-functionlized Kapton (left) and dienophile-fucntionalized polished aluminum (right) before (top) and after (bottom) peeling at ambient temperature.

XPS analysis revealed that the peeling induces a strong modification of the elemental composition of the diene functionalized Kapton surface with the decrease of the silicon content (from 7 to 2 at %) that might be related to the partial loss of the plasma copolymer layer. An accompanying change in the XPS C1s envelope of the peeled diene surface is also evident as it can be observed that the general curve shape is clearly close to the native Kapton one, with in particular the presence of the $\pi-\pi^*$ shake-up satellite related to the Kapton aromatic structures. After a calibration step according to the N1s position at 400.6 eV (i.e., imide bond), the C1s spectra

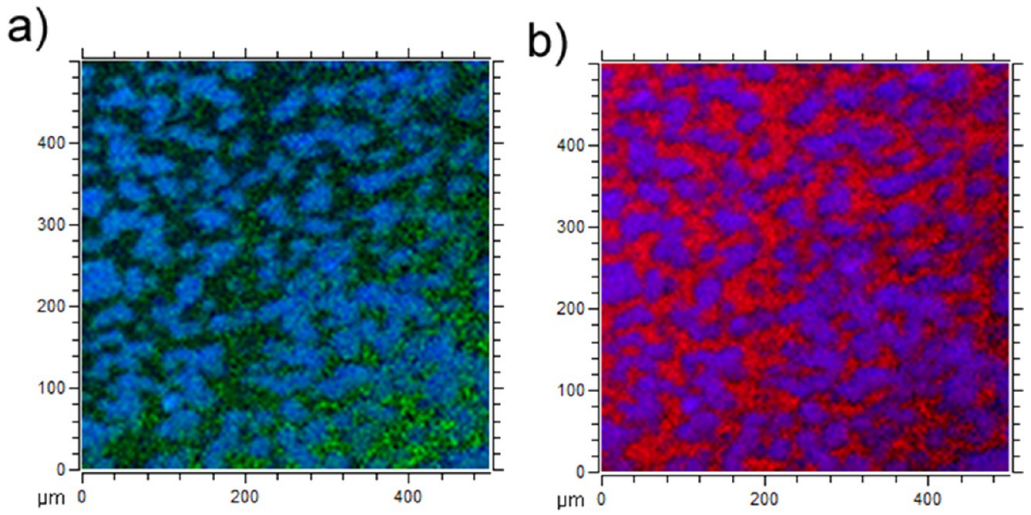

Figure 12. ToF-SIMS cartographies of the dienophile/aluminum surface after peeling: (a) overlay of $C_6H_7O^+$ (blue) and $C_3H_2N_2O_2^+$ (green) ions and (b) overlay of $SiOH^+$ (red) and $C_6H_7O^+$ (blue) ions.

could be fitted with 5 different carbon functionalities: namely C═C at 284.7 eV, C*═C−C(O)/C−N/C*−C(O)−N at 285.7 eV, C−O at 286.3 eV, C═O/O═C−N at 287.7 eV, and O═C−N−C═O at 288.6 eV. Compared to the native Kapton C1s signal, one can notice the apparition of a new contribution at 287.7 eV. Additionally, a good convergence in the C1s curve fit was only possible for a FWHM of the C−O contribution around 1.5 eV, while this value was around 1 eV for the native Kapton C1s; this suggests that this 286.3 contribution cannot solely contain C−O bonds but maybe also C*−NH−C═O bonds. In conclusion, it appears that the diene-functionalized Kapton surface after peeling is composed of Kapton and some plasma polymer residues.

By considering the XPS elemental composition of the dienophile-functionalized aluminum surface before and after peeling, no major difference can be noted as the layers present similar elemental C, O, Si, and N content. However, the XPS C1s general shape of the dienophile-Al surface after peeling does not look like the original dienophile aluminum surface. The presence of a small shake-up fingerprint at 291.3 eV suggests the presence of Kapton, meaning that the locus of failure should be located inside the Kapton substrate; the small analysis depth of XPS (a few nanometers) suggests that the lamination occurred not deeply inside Kapton, as otherwise suggested by the C1s environment of the diene functionalized Kapton surface after peeling. Finally, it was not possible to obtain a satisfactory C1s curve fitting by applying exactly the same parameters exploited for the C1s diene functionalized layer (notably, the FWHM was around 1.5 eV against 1.0 eV). Hence, it can be concluded that a mixed failure mechanism (adhesive and cohesive in the Kapton) was at the origin of an heterogeneous morphology (Figure 11) and chemistry of the peeled dienophile functionalized surface (XPS results).

Complementary ToF-SIMS analyses were carried out on the peeled surfaces to retrieve more precise chemical and molecular information with 2D spatial resolution. For that purpose, in a first step, native Kapton, diene functionalized Kapton and dienophile functionalized aluminum were analyzed to detect some characteristic peaks of the different surfaces. Hence, both diene and dienophile surfaces presented a peak at m/z = 44.97 that can be attributed to the $SiOH^+$ fragment coming from the MA-VTMOS plasma layer. A m/z = 95.06 ion was detected in the diene surface and might be related to the methylfurfuryl cation, $C_6H_7O^+$. Finally, both native Kapton and diene surface presented a peak at m/z = 98.01 that might correspond to a $C_3H_2N_2O_2^+$ fragment. One has first to report that ToF-SIMS of any peeled layer never showed the Al^+ (or Al compound) signal, implying that delamination did not occur at the Al surface.

Cartographies were constructed by attributing the red, blue and green colors to the following $SiOH^+$, $C_6H_7O^+$, $C_3H_2N_2O_2^+$ ions respectively. Figure 12a presents such a ToF-SIMS cartography resulting from the overlay of the $C_6H_7O^+$ (blue) and $C_3H_2N_2O_2^+$ (green) ions of the dienophile (on aluminum) surface after peeling. As the green color is representative of both diene and Kapton, a perfect overlap of the blue (diene, only) and green zones should allow to conclude to the exclusive and sole presence of a diene layer. However, here, blue zones and green islands can be observed indicating the presence of diene and Kapton, respectively, at different loci of failure. This latter result is fully in agreement with the XPS C1s peak containing the shake-up which is absolutely characteristic of the Kapton substrate. By considering Figure 12b, overlaying the $SiOH^+$ (red) and $C_6H_7O^+$ (blue) signals, some magenta and red zones can be observed. The magenta color results from the overlap of the red and blue colors (as the signal intensity of the corresponding ions is similar); these magenta zones are undoubtedly to be attributed to a diene layer; as a consequence, it can be deduced that the red zone corresponds to the dienophile layer. One can notice that the shapes and positions of the different blue zones in Figure 12.a are perfectly similar to the magenta ones of Figure 12.b, thus, confirming the attribution of these zones to the diene layer. In the same way, the shapes and positions of the black zones in Figure 12.a perfectly fitted with the red zones of Figure 12.b. Hence, according to XPS and ToF-SIMS analyses, it can be concluded that the dienophile/aluminum layer after peeling is composed of dienophile, diene, and Kapton residues.

A debonding property was measured when the functionalized aluminum and Kapton laminate was submitted to a thermal treatment. This phenomenon is illustrated in Figure 13, presenting the metal−polymer peel strength as a function of the peeled length during different heating/cooling cycles. Hence, when the system was simply heated up to 200 °C over a

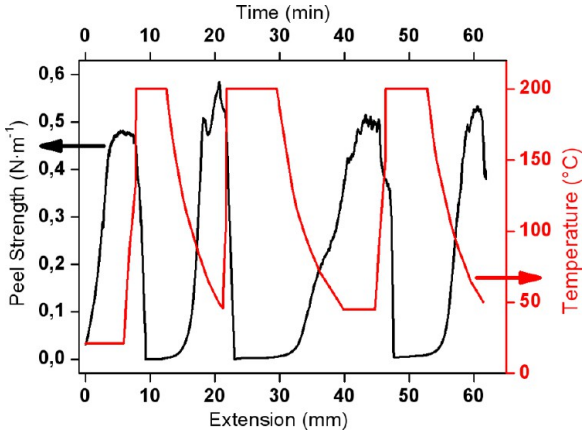

Figure 13. Functionalized Kapton-aluminum peel strength as a function of peel length during heating/cooling cycles.

few minutes, the peel strength value rapidly drops to zero. During the cooling, the peel strength increased again until reaching the mean value of 0.6 N/mm allowing to clearly establish the thermally responsive adhesion property of the system.

By comparing AFM and SEM images acquired on the same dienophile surface after peeling at 200 °C (Figure 14), it appeared that the bright zones in SEM corresponded to dark zones in AFM with the lower height. The sample height profiles across the border of various zones revealed systematically a 20 nm height difference, which can be attributed to the 20 nm thickness of the diene or the dienophile layer. However, as both FT-IR and ToF-SIMS analyses revealed that the failure never occurred at the aluminum-dienophile layer interface (as an organic coating was always detected and no Al^+ ion was never detected), it can be concluded that this difference height can be related to some diene layers delaminated from functionalized kapton and glued to the dienophile-functionalized aluminum, whereas the bright zones can correspond to "free" dienophile surface. By using the ImageJ software, the free dienophile area was estimated to cover around 50% of the total area, allowing to conclude that the rDA has efficiently occurred at the solid functionalized surfaces.

4. CONCLUSION

A new dry atmospheric procedure based on plasma surface functionalization and gas phase reactions, involving simple compounds readily available commercially, has been developed to graft diene and dienophile groups onto a large variety of substrates, metallic or polymer ones such as PEN or Kapton foils. Hence, strong polymer−polymer and polymer−metal adhesion based on chemical Diels−Alder reactions was achieved with peel strengths higher than the cohesive strength in polymer (PEN or Kapton). Interestingly, it is worth noting that by applying the same procedure, higher adhesive joints in polymer−metal laminates can be reached by changing the polymer nature and/or using a substrate presenting an important viscoelastic property.

Additionally, it has been observed that the functionalized polymer−metal assemblies presented a thermally responsive

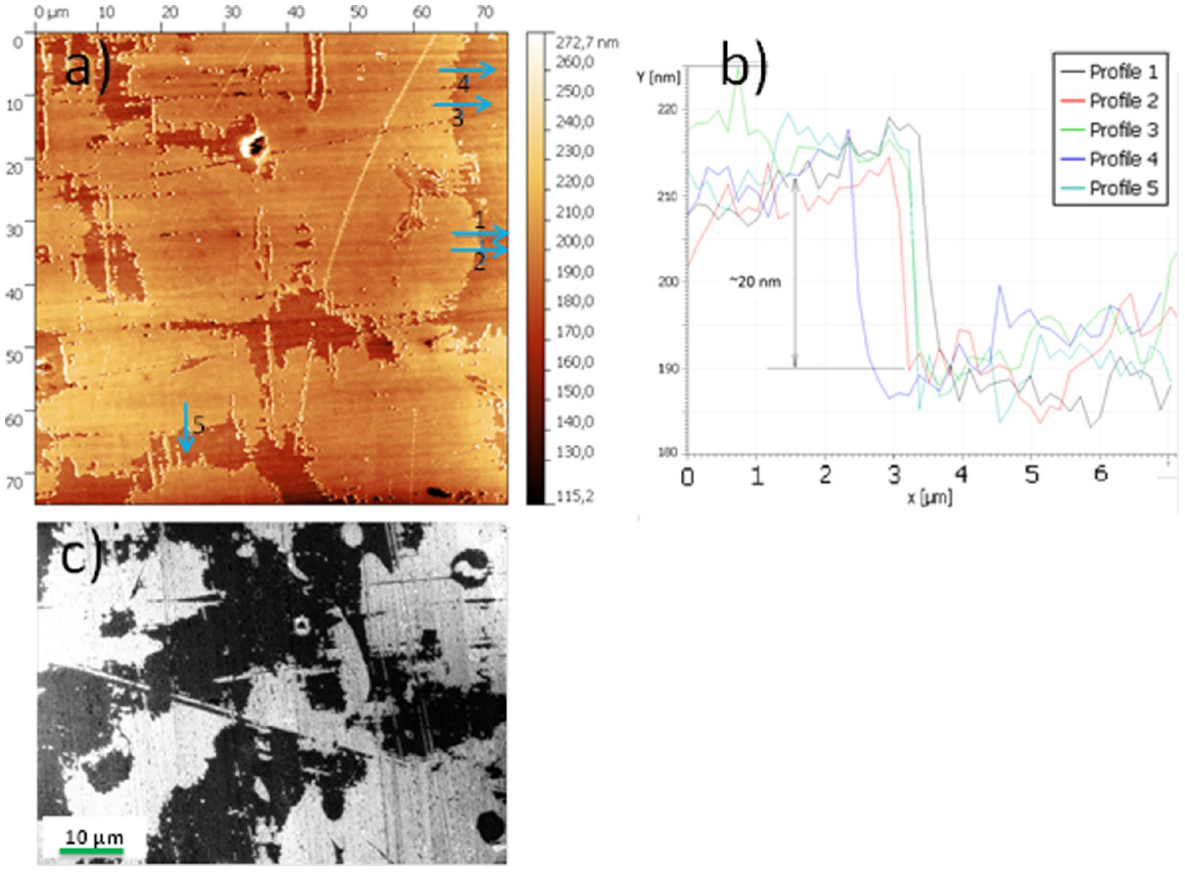

Figure 14. (a) AFM 3D cartography, (b) sample height profile retrieved from the AFM image, an (c)d SEM picture of the dienophile functionalized aluminum after peeling at 200 °C.

adhesion property as the peel strength drastically decreased by a factor of 50 when the system was submitted to a 200 °C heating. At least, four heating/cooling cycles were carried out and led systematically to peel strengths of 0.01 or 0.5 N/mm, respectively.

Finally, the procedure developed might be tailored to a large variety of applications, as it is possible to tune the temperature at which the adhesive property occurs. For that, particular diene and dienophile compound structures have to be selected as it is now well-established that the location of electron-withdrawing or electron-donating groups in the structure is directly connected to the temperatures for the DA and retro-DA reactions.

AUTHOR INFORMATION

Corresponding Author

*E-mail: moreno@lippmann.lu.

Author Contributions

All authors have given approval to the final version of the manuscript.

Notes

The authors declare no competing financial interest.

ACKNOWLEDGMENTS

This research was carried out in the framework of the REVAD project funded by the Luxembourgish "Fonds National de la Recherche" (FNR). The authors thank J. Didierjean and Dr. J. Guillot for XPS analysis. Dr. G. Frache and M. Gérard are also grateful acknowledged for ToF-SIMS analyses and mechanical engineering, respectively.

REFERENCES

(1) Murphy, E. B.; Wudl, F. *Prog. Polym. Sci.* **2010**, *35*, 223−251.
(2) Guimard, N. K.; Oehlenschlaeger, K. K.; Zhou, J.; Hilf, S.; Schmidt, F. G.; Barner-Kowollik, C. *Macromol. Chem. Phys.* **2012**, *212*, 131−143.
(3) Sanyal, A. *Macromol. Chem. Phys.* **2010**, *211*, 1417−1425.
(4) Nishida, H. *Polym. J.* **2011**, *43*, 435−447.
(5) Tasdelen, M. A. *Polym. Chem.* **2011**, *2*, 2133−2145.
(6) Chen, J.-S.; Ober, C. K.; Poliks, M. D. *Polymer* **2002**, *43*, 131−139.
(7) Liu, Y.-L.; Hsieh, C.-Y.; Chen, Y.-W. *Polymer* **2006**, *47*, 2581−2586.
(8) Aubert, J. H. *J. Adhes.* **2003**, *79*, 609−616.
(9) Kim, J.; Park, W.; Hong, H. *Bull. Korean Chem. Soc.* **2004**, *25*, 1081−1084.
(10) Chan, E. W.L.; Yousaf, M. N.; Mrksich, M. *J. Phys. Chem. A* **2000**, *104*, 9315−9320.
(11) Siffer, F.; Schultz, J.; Roucoules, V. In *Adhesion: Current Research and Applications*; Possart, W., Ed.; Wiley−VCH: Weinheim, Germany, 2006; pp 289−303.
(12) Siffer, F. La fonctionnalisation de surface par polymérisation plasma: une nouvelle stratégie d'élaboration de matériaux à pouvoir adhésif réversible. *Ph.D. Thesis*, University of Haute-Alsace, Mulhouse, France, Dec 2006.
(13) Teare, D. O. H.; Schofield, W. C. E.; Garrod, R. P.; Badyal, J. P. S. *J. Phys. Chem.* **2005**, *109*, 20923−20928.
(14) Cosnier, F.; Celzard, A.; Furdin, G.; Bégin, J D.; Marêché, F.; Barrès, O. *Carbon* **2005**, *43*, 2554−2563.
(15) Zhang, M.; Zhao, J.; Gao, L. *Sens. Actuators, A.* **2008**, *141*, 213−216.
(16) Sun, G.; Hovest, M.; Zhang, X.; Hinrichs, K.; Rosu, D. M.; Lauermann, I.; Zielke, C.; Vollmer, A.; Löchel, H.; Ay, B.; Holzhütter, H.-G.; Schade, U.; Esser, N.; Volkmerb, R.; Rappich, J. *Surf. Interface Anal.* **2011**, *43*, 1203−1210.
(17) Chen, G.; Gupta, M.; Chan, K.; Gleason, K. K. *Macromol. Rapid Commun.* **2007**, *28*, 2205−2209.
(18) Tarducci, C.; Badyal, J. P. S.; Brewer, S. A.; Willis, C. *Chem. Commun.* **2005**, 3, 406−408.
(19) Roucoules, V.; Siffer, F.; Ponche, A.; Vallat, M. F. In *Proceedings of the 31st Annual Meeting of The Adhesion Society*; Austin, USA, February 2008.
(20) Gandini, A. *Prog. Polym. Sci.* **2013**, *37*, 1−29.
(21) Evenson, S. A.; Fail, C. A.; Badyal, J. P. S. *Chem. Mater.* **2010**, *12*, 3038−3043.
(22) Manakhov, A.; Moreno-Couranjou, M.; Boscher, N. D.; Rogé, V.; Choquet, P.; Pireaux, J.-J. *Plasma Processes Polym.* **2012**, *9*, 435−445.
(23) Manakhov, A.; Moreno-Couranjou, M.; Choquet, P.; Boscher, N. D.; Pireaux, J.-J. *Surf. Coat. Technol.* **2011**, S466−S469.